Phys. Status Solidi A **211,** No. 2, 288–293 (2014) / **DOI** 10.1002/pssa.201330053

physica status solidi pss a
www.pss-a.com
applications and materials science

Statistical characterization of self-assembled charged nanoparticle structures

G. Zvejnieks*, V. N. Kuzovkov, and E. A. Kotomin

Institute of Solid State Physics, University of Latvia, Kengaraga str. 8, 1063 Riga, Latvia

Received 18 June 2013, revised 4 September 2013, accepted 4 September 2013
Published online 14 October 2013

Keywords nanoparticles, nanostructures, reverse Monte Carlo method, self-assembly

* Corresponding author: e-mail guntars@latnet.lv, Phone: +371-67187480, Fax: +371-67132778

We propose a novel approach for description of dynamics of nanostructure formation for a system consisting of oppositely charged particles. The combination of numerical solution of analytical Bogolyubov–Born–Green–Kirkwood–Yvon (BBGKY) type equation set with reverse Monte Carlo (RMC) method allows us to overcome difficulties of standard approaches, such as kinetic Monte Carlo or Molecular Dynamics, to describe effects of long-range Coulomb interactions. Moreover, this allows one to study the system dynamics on realistic time and length scales. We applied this method to a simple short-range Lenard–Jones (LJ)-like three- (3D) and two-dimensional (2D) system combining the long-range Coulomb and LJ interactions. As expected, the nanoparticle growth driven by the Ostwald ripening is observed in the former case, while long-range interaction limited self-assembled nanostructures are observed in the latter case.

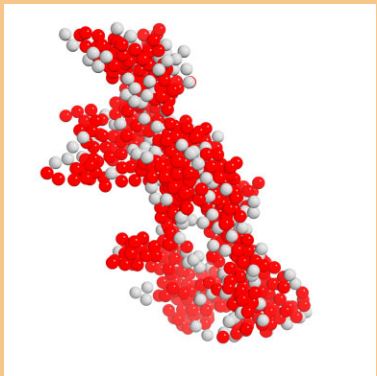

Example of 3D structure of self-assembled nanoparticles interacting via short-range LJ and long-range Coulomb potentials obtained by improved reverse Monte Carlo simulations.

1 Introduction Description of pattern formation formed by oppositely charged cationic and anionic molecules on surfaces and in a bulk is of a particular interest *e.g.*, in electrochemistry and biophysics. In turn, such patterns may affect the surface/interface (catalytic) properties. For example, surfaces with ionic components could be modified without mechanical treatment. Moreover, in dense surface systems charged molecules show a large variety of patterns, that depend on ionic strength.

Attempts to use traditional approaches in a study of dynamic, non-equilibrium properties of nanoparticle (NP) systems have shown a very limited success due to long relaxation times needed for a system ordering. Additional problems arise in systems of charged NP due to the long-range NP interactions [1]. Thus, studies of ionic systems were mainly performed in the limit of high salt concentration (strong screening) when the long-range Coulomb potential is traditionally replaced by a short-range Yukawa potential [2, 3].

To handle this problem, we demonstrate here the potential of the integrated approach that includes: (i) analytical part [4] (introduction of kinetic self-consistent equations for radial distribution functions), (ii) the numerical part (solution of these equations by obtaining radial distribution functions), and (iii) change of radial distribution representation to real space particle distribution (transformation of information). In the latter case, partial structure factors and characteristic system snapshots obtained by the reverse Monte Carlo (RMC) are determined through the radial distribution functions. We have succeeded in kinetic calculations for ionic system up times that are four orders of magnitude longer than those in a conventional method of

Brownian dynamics. Within the extended time scale free NPs are able to diffuse at distances of the order ~3000 NP diameters. We present the results for two- (2D) [5] and three-dimensional (3D) ionic systems.

2 Method We study both the kinetics of pattern formation and phase separation in a system of two types of oppositely charged molecules (*e.g.*, *A* and *B*) with competing short- and long-range interactions on surfaces/interfaces. The molecular ordering occurs on the background of the Ostwald ripening and thus is strongly non-equilibrium.

2.1 Kinetic equations The complete set of coupled kinetic equations for particle many-body densities is similar to the Bogolyubov–Born–Green–Kirkwood–Yvon (BBGKY) hierarchy and given by [4]

$$\frac{\partial \eta_{\alpha\beta}(r,t)}{\partial t} = D_{\alpha\beta}\nabla\left[\nabla\eta_{\alpha\beta}(r,t) + \frac{\eta_{\alpha\beta}(r,t)}{k_{\mathrm{B}}T}\nabla W_{\alpha\beta}(r)\right], \tag{1}$$

where subscripts α and β denote different sorts of particles. These equations describe the particle diffusion, D, in potentials of mean forces W that are functionals of the correlation functions $\eta(r,t)$ (CF) at distance r and time t. Here k_{B} is Boltzmann constant and T temperature. In particular, for simple two component systems we obtain three time-dependent CF where we denote the similar particle CF as X_{AA} and X_{BB}, while dissimilar CF by Y_{AB}. These functions are sufficiently smooth (when solving analytical non-linear equations numerically) and they can be used in further transformations (Fourier, etc.).

The set of Eq. (1) coincide with the first exact equations based on many-body theory while effective potentials of mean forces are obtained approximately. We used two approximations: (i) Coulomb interaction contribution in the potentials of mean forces is found in a standard way for Coulomb systems by solution of Poisson equation, where charge density is written in the terms of CF [4]. (ii) Contribution of short-range interactions [4] is found in the Kirkwood approximation [6] known in the statistical physics of condensed systems. For equilibrium systems this approximation along with other hypernetted-chain or Percus–Yevick type approximations defines the group of self-consistent approximations used in development of semi-quantitative theories. However, for non-equilibrium systems the last approximations are inapplicable since they contradict to the structure of kinetic equations.

Strictly speaking, the accuracy of analytical theories can be established either by a comparison with exact solutions or the results of reliable Monte Carlo simulations. However, there are no exact solutions for the considered systems in both equilibrium and non-equilibrium cases, while the method of Monte Carlo has considerable restrictions. So, for the systems with both long-range interactions and long-range correlations the Monte Carlo calculations are quite time consuming leading to a rather short simulation times that are far from the experimentally relevant time scale. Contrary, in the proposed approach we considerably exceed the typical Monte Carlo simulation times for Coulomb systems and thus a direct comparison of obtained results is impossible. However, note the studies of systems with short-range interactions and chemical reactions [7, 8]. It was shown that chemical reactions lead to non-equilibrium critical phenomena that in turn form long-range correlations. It was demonstrated by a comparison of a large number of examples with Monte Carlo results, that Kirkwood superposition approximation leads to *exact values* of nontrivial critical exponents describing kinetics.

The set of coupled kinetic equations Eq. (1) is solved numerically by discretizing them and by using a standard recurrent procedure for non-linear terms [4]. The drawback, however, is that solution is given in a form of correlation functions that contain quite an abstract information (distance dependent distribution of particle pairs). In turn, usually in pattern formation we are interested in single particle distributions in a real space. Thus, a mapping of information from correlation functions into characteristic snapshots is required.

2.2 Reverse Monte Carlo approach The RMC method [4, 9, 10] is used to transform the radial distribution functions (*e.g.*, obtained in many-particle density formalism) to a particular microscopic *A* and *B* molecule distribution in a real space. An advantage of the RMC is the needless of inter-particle interaction definition. Instead, the problem is reduced to achieving the best possible coincidence between the RMC modeled and theoretically or experimentally obtained test functions. The coincidence is controlled by goodness of fit statistical model

$$\chi^2 = \sum_{i=1}^{n} F_i \frac{\left(O_i - O_i^0\right)^2}{O_i^0}, \tag{2}$$

where O_i is the observed test function frequency in RMC, while O_i^0 is provided by theoretical or experimental data. Here, we propose *an improved* RMC by introducing an additional scaling function F_i that increases the significance of extrema points in the χ^2 summation.

The change of χ^2 is modeled by randomly selecting a particle and generating new spatial coordinates. Then the test function values O_i are recalculated and new χ'^2 value is obtained. Next, two scenarios are possible: (i) In the standard RMC method a *reversible* scheme can be used, when the particle move is accepted instantly if $\chi'^2 < \chi^2$ or with probability $\exp\left(-\left(\chi'^2 - \chi^2\right)/2\right)$ if $\chi'^2 > \chi^2$. (ii) Alternatively, one can use *irreversible* scheme, when particle moves are accepted only if $\chi'^2 < \chi^2$.

3 Results In order to avoid finite size effects, the RMC system is always selected at least several times larger that the length of numerically calculated CF. Simulations start with

random distribution of particles A and B corresponding to their concentration used in numerical calculations.

3.1 RMC simulations of 3D systems Application of the standard RMC method [9] for modeling 3D correlation functions is shown in Fig. 1. Note that RMC method uses neither such physical parameters as temperature, nor NP interaction potentials. In turn, the method compares two distributions of NPs by means of the correlation functions. The first one is found by solving the set of kinetic equations Eq. (1), while the second is generated by RMC. System energy is not required. The convergence of RMC method is determined by the detailed shape of correlation functions (see below) obtained from Eq. (1) and thus it indirectly depends on the selected physical parameters.

A simple system with short-range interaction described by the Lenard–Jones (LJ) potentials without Coulomb interactions is shown in Fig. 1. The LJ potential contains two parameters: the NP diameter, r_0, and the energy parameter, U_0 [4]. The potential assumes nanoparticle repulsion at short distances, $r < r_c = 2^{1/6} r_0$ (due to finite nanoparticle sizes) and attraction at larger distances, $r > r_c$. Finally, in our binary system for similar nanoparticles we include both (attractive and repulsive) terms of LJ potential while for dissimilar particles we retain only the first, repulsive LJ term. Thus, without Coulomb interactions dissimilar NPs A and B just repel each other, whereas similar NPs attract each other and thus could aggregate.

Let us note that the same model using different methods was considered earlier, see *e.g.*, [11, 12]. Molecular dynamics methods were used there to solve reversible equation of motion (Newton dynamics). However, our approach is based on irreversible equations of motion (Brownian dynamics) where NPs are characterized by partial diffusion coefficients while an unperturbed particles perform random walks. The latter is closer to experimental situation for NPs in solutions, where they are surrounded by other smaller particles. In other words, we derive the kinetic equations on a basis of stochastic differential equations describing the time evolution on a *subset* degrees of freedom. The subset typically contains collective (macroscopic) variables that vary slowly contrary to other (microscopic) variables of the system. The latter are responsible for the stochastic nature of the Brownian dynamics. It should be stressed that we study the kinetics of systems far from equilibrium, when the energy minimum principle either is inapplicable (*e.g.*, when charged particles might experience chemical reactions [13]) or is applicable only asymptotically.

The system is characterized by dimensionless concentration $n = (n_A + n_B) r_0^3 = 0.2$ and temperature $\theta = k_B T / U_0 = 0.7$. Physically, the considered system corresponds to liquid-like state, where two sorts of NPs create aggregates whose ordering depends on the temperature. We provide here the results for different times, t (in the units of diffusion time $t_0 = r_0^2/D$): $t = 2^{16}$, Fig. 1(a–c) and $t = 2^{20}$, Fig. 1(d–f).

The standard RMC recovers well liquid- or gas-like spatial particle structures, when CF values are close to unity (no strong spatial correlation, Poisson distribution). However, the standard RMC fails for more dense and well-ordered structures that are characterized by CF values strongly

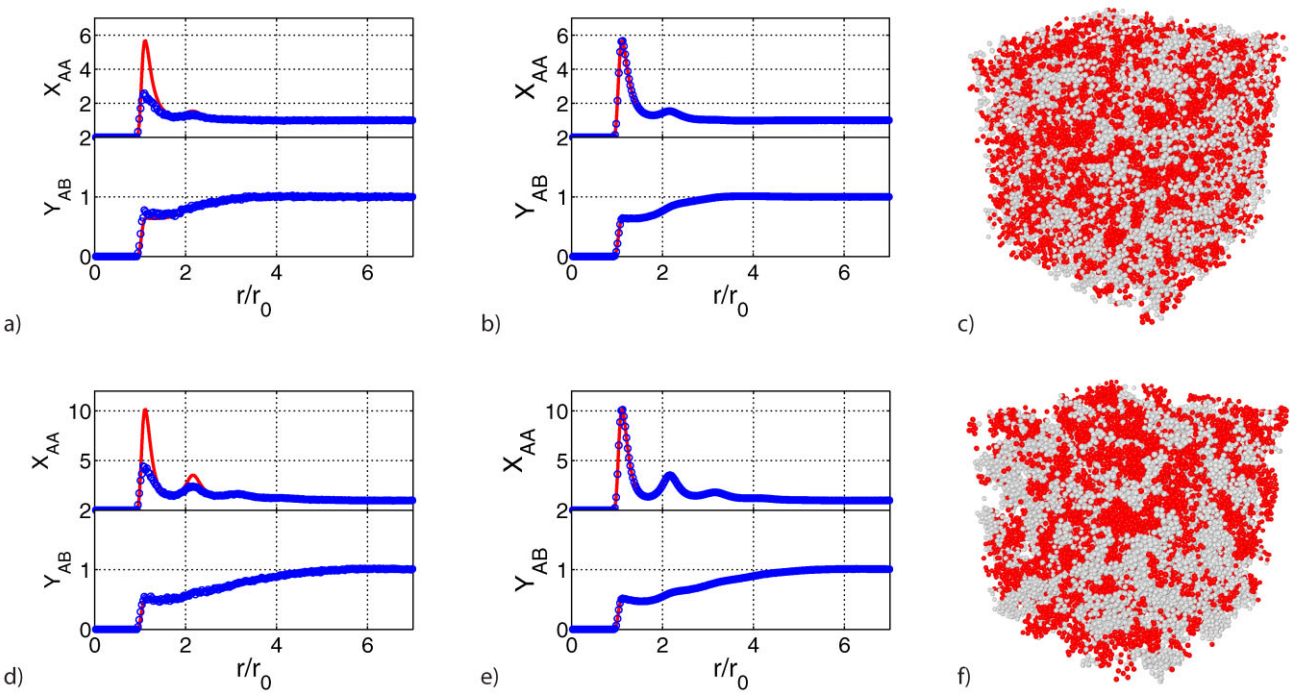

Figure 1 Comparison of standard RMC method (a) and (d) with improved RMC (b) and (e) for 3D system. Correlation functions are marked by line and circles for theoretical and RMC results, respectively. The CF deviation from the unity means development of spatial correlations. The snapshots obtained by improved RMC are given in (c) and (f).

deviating from unity. This is connected to the fact that CF extrema usually consist of a limited number of points whose contribution in χ^2 sum are negligible in a comparison with the total number of CF data points. Despite the built in $\chi^2(F_i = 1)$ function relative scaling assumption for such cases, it turns out to be insufficient. In turn, an introduction of additional amplification for CF extrema, $\chi^2(F_i \neq 1)$, in improved RMC method allows us to find the spatial particle distribution function, that agrees more closely with the theoretical one.

Agreement between theoretical and RMC-simulated CF curves strongly affects the visualized system snapshots. In the case of the standard RMC method, the recovered spatial distributions are biased toward less ordered state (RMC CF are closer to unity than theoretical one). This, in turn, hinders the appearance of ordered structures. Contrary, the improved RMC Fig. 1c, f allows us to monitor the kinetics of system behavior with high spatial resolution and accuracy.

By keeping the same interaction potentials as in Fig. 1 case, the self-assembling of nanoparticles can be observed at longer times $t = 2^{24}$. In this case the numerical solution leads to crystal-like CF that considerably exceeds unity, Fig. 2. The improved RMC method now recovers the striped particle spatial distribution, Fig. 2b. The new spatial representation of CF allows us to obtain qualitatively new information of the system, *e.g.*, cluster distribution function, $F(s) = N_s \langle s \rangle^2 / \Theta$, where Θ denotes the particle A or B concentration, $\langle s \rangle$ is average cluster size, and N_s the cluster density of size s. It should be stressed that it is impossible to obtain the cluster distribution directly from CF.

In contrast to discrete case, when clusters can be easily defined, *e.g.*, as particles occupying the nearest neighboring (NN) positions, the continuous case requires a NN definition. Here we define NN as particles which are separated closer than $r/r_0 < 2^{1/6}$. In this case, cluster distribution function shows no dominating cluster size but existence of a large number of small clusters with exponentially decreasing number of large clusters.

3.2 RMC simulations of 2D systems The results of the Section 3.1 for 3D structures could be generalized for the case of LJ potential combined with Coulomb interaction, see *e.g.*, snapshot in Abstract. However, in order to demonstrate the versatility of the proposed approach, let us consider the effect of Coulomb interaction for 2D system.

Similarly to 3D case, in order to describe the crystal-like CF structures with extrema that deviates strongly from unity, a rescaling of $\chi^2(F_i \neq 1)$ is required.

Contrary to Figs. 1 and 2, we consider a 2D system, where short-range LJ potential is complemented with long-range Coulomb interactions. As in 3D case, similar particles have a tendency to create aggregates. However, contrary to pure LJ case, now the aggregate (domain) growth is *limited*, their sizes are stabilized, while the Coulomb interaction "glues" oppositely charged domains. As a result, a complicated labyrinth-like structures emerge, where dissimilar particle domains interchange. Unlike a 3D system, the system ordering in 2D-snapshots can be followed more easily in all details. The calculated correlation functions and corresponding RMC lattice snapshot time development are shown in Fig. 3(a–c) and (d–f), respectively.

We performed the improved RMC simulations in two steps. First, we performed the reversible RMC simulations until the χ^2 convergence is reached, see a horizontal slope region in Fig. 4. In this case, further decrease of χ^2 is hindered by the reversible algorithm step, when energetically unfavorable states are accepted with a certain probability, *i.e.*, there is a "temperature" effect. The number of iterations needed to reach the convergence state depends on the complexity of correlation functions. For a simple liquid-like structures with a small correlation length one needs the smallest number of iterations, see Fig. 4 [line (a)]. However, the number of required iterations increases, when correlation functions approach a crystal-like state, when these functions contain pronounced extremes, see Fig. 4 [lines (b) and (c)]. Next, we used the irreversible RMC scheme (starting from positions indicated by arrows in Fig. 4), to obtain the final results. This is characterized by a further step-like decrease

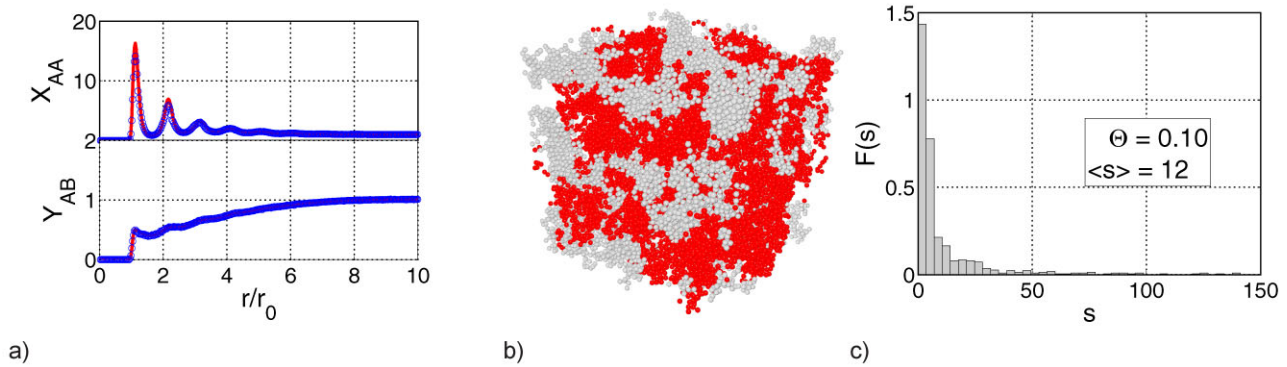

Figure 2 Example of improved RMC method application to analysis of late times (ordered structure) CF case (a). Theoretical CF functions are marked by line and improved RMC by circles, respectively. The striped spatial particle distribution snapshot (b). Cluster analysis (c).

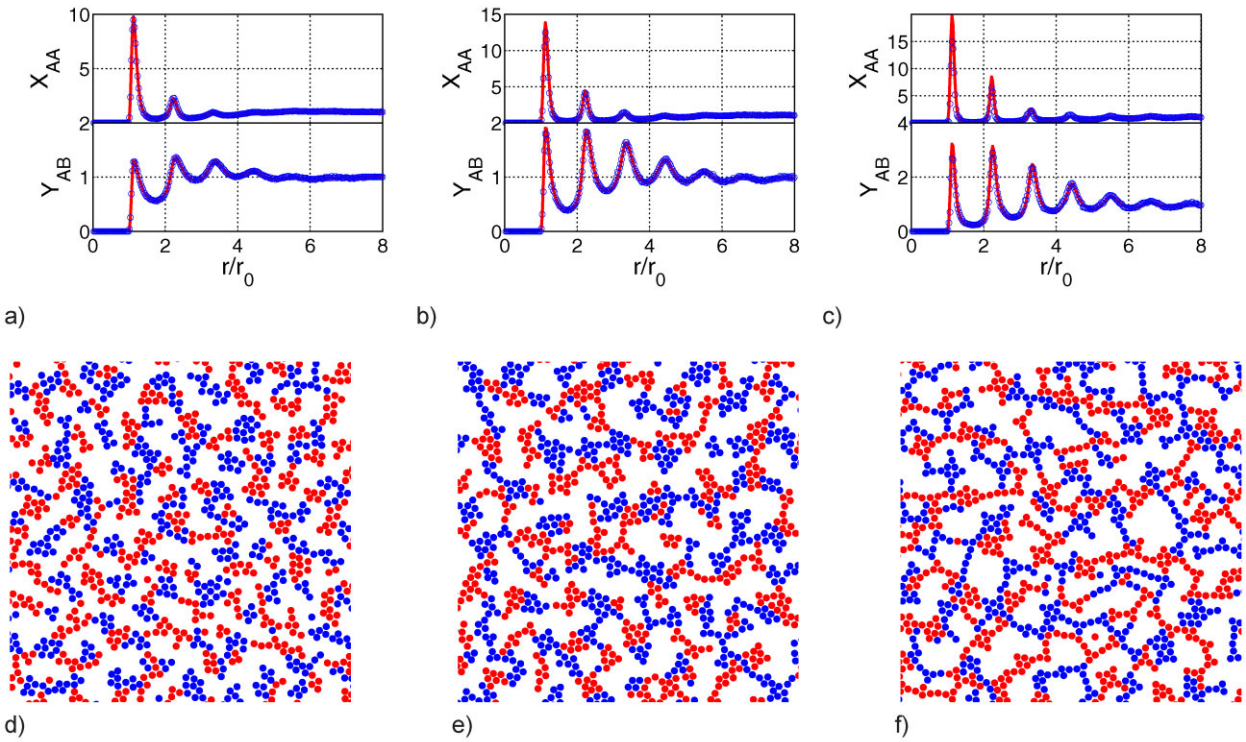

Figure 3 Theoretical (curves) and improved RMC simulated (circles) correlation functions for 2D systems at different times (a–c) and corresponding fragments of lattice snapshots (d–f).

of χ^2 parameter. The irreversible simulations could be performed infinitely long, which, in turn, takes more computational time. Therefore, we stoped simulations after the χ^2 criteria show a slowing down tendency. In these regimes, continuation of simulations has a little effect on agreement between theoretical and RMC CFs, as well as the spatial particle distribution.

By comparing the effect of irreversibility in reducing χ^2, one can notice that the largest effect occurs for the most disordered state, while the smallest effect for the most ordered (largest CF maximums around 20) state. By reversing the problem and starting from assumption that at "absolute zero temperature" (irreversible RMC regime when only χ^2 decreasing configurations are accepted) identical "temperature" increase (reversible RMC regime when χ^2 increasing configurations might be accepted) has the dominant effect on small scale structures. Small clusters are rather easy to melt than large scale crystal-like structures, since less bonds need to be broken.

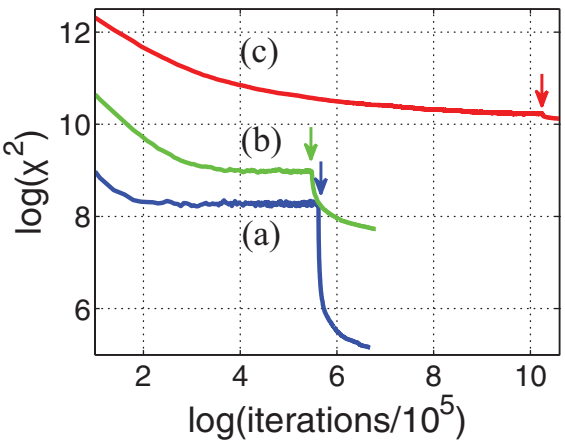

Figure 4 Consecutive application of reversible- and irreversible (marked by arrows) improved RMC method in 2D case. Curves (a–c) reflect CF development in time and correspond to Fig. 3(a–c).

4 Summary We proposed here a novel method that combines the analytical formalism of the joint correlation functions and the RMC method to monitor and visualize pattern formation processes of charged nanoparticles. We provided illustrations that demonstrate the method ability in different short- and long-range particle interaction limits, in 2D and 3D systems. For system with only short-range interactions, we observed the well known Ostwald ripening type behavior of unlimited aggregate growth of attracting particles. However, when the short-range LJ type potential is complemented by the long-range Coulomb potential, the nanoparticle self-assembling tends toward an equilibrium in a binary systems of oppositely charged molecules adsorbed at a surface or at an interface. Thus, the statistical analysis of a particle segregation into clusters is an alternative approach to the standard kinetic Monte Carlo or molecular dynamics simulations.

Acknowledgements This work was supported by Latvian grant 237/2012.

References

[1] D. A. Walker, B. Kowalczyk, M. Olvera de la Cruz, and B. A. Grzybowski, Nanoscale **3**, 1316 (2011).
[2] R. Orlik, A. C. Mitus, B. Kowalczyk, A. Z. Patashinski, and B. A. Grzybowski, J. Non-Cryst. Solids **355**, 1360 (2009).
[3] R. Zhang, P. K. Jha, and M. Olvera de la Cruz, Soft Matter **9**, 5042 (2013).
[4] V. N. Kuzovkov, G. Zvejnieks, E. A. Kotomin, and M. Olvera de la Cruz, Phys. Rev. E **82**, 021602 (2010).
[5] V. N. Kuzovkov, E. A. Kotomin, and G. Zvejnieks, J. Phys. Chem. B **115**, 14626 (2011).
[6] J. G. Kirkwood, J. Chem. Phys. **3**, 300 (1935).
[7] E. A. Kotomin and V. N. Kuzovkov, Modern Aspects of Diffusion-Controlled Reactions: Cooperative Phenomena in Bimolecular Processes, Vol. 34: Comprehensive Chemical Kinetics (Elsevier, North Holland, Amsterdam, 1996).
[8] E. A. Kotomin and V. N. Kuzovkov, Rep. Prog. Phys. **55**, 2079 (1992).
[9] R. L. McGreevy and L. Pusztai, Mol. Sim. **1**, 359 (1988).
[10] R. L. McGreevy, J. Phys.: Condens. Matter **13**, R877 (2001).
[11] S. Loverde, F. Solis, and M. Olvera de la Cruz, Phys. Rev. Lett. **98**, 237802 (2007).
[12] S. Loverde and M. Olvera de la Cruz, J. Chem. Phys. **127**, 164707 (2007).
[13] V. N. Kuzovkov, E. A. Kotomin, and G. Zvejnieks, J. Chem. Phys. **135**, 224503 (2011).